Available online at www.sciencedirect.com
SCIENCE DIRECT®
Journal of Computational Physics 200 (2004) 639–653
JOURNAL OF COMPUTATIONAL PHYSICS
www.elsevier.com/locate/jcp

On the computation of steady Hopper flows II: von Mises materials in various geometries

Pierre A. Gremaud [a,*,1], John V. Matthews [b,2], Meghan O'Malley [a]

[a] *Department of Mathematics and Center for Research in Scientific Computation, North Carolina State University, Box 8205, Raleigh, NC 27695-8205, USA*
[b] *Department of Mathematics, Duke University, Durham, NC 27708-0320, USA*

Received 9 December 2003; received in revised form 23 April 2004; accepted 23 April 2004
Available online 24 June 2004

Abstract

Similarity solutions are constructed for the flow of granular materials through hoppers. Unlike previous work, the present approach applies to nonaxisymmetric containers. The model involves ten unknowns (stresses, velocity, and plasticity function) determined by nine nonlinear first order partial differential equations together with a quadratic algebraic constraint (yield condition). A pseudospectral discretization is applied; the resulting problem is solved with a trust region method. The important role of the hopper geometry on the flow is illustrated by several numerical experiments of industrial relevance.

Keywords: Elliptic; Granular; Similarity; Spectral

1. Introduction

This is the second in a series of papers on the mechanics of a granular material under the influence of gravity flowing through converging hoppers of simple geometry. While such devices are common in many industrial processes, the withdrawal of stored materials from hoppers and bins is well known to be problematic. Segregation, lack of flow, flooding (uncontrolled flow) and structural failures are often encountered [14]. A better understanding of such flows should lead to improved hopper design criteria.

Commonly used models are subject to severe restrictions [8,10,12,13,16,22,24]:

* Corresponding author. Tel.: +1-919-515-5289; fax: +1-919-515-1636.
E-mail addresses: gremaud@math.ncsu.edu, gremaud@unity.ncsu.edu (P.A. Gremaud), jvmatthe@math.duke.edu (J.V. Matthews), msomalle@unity.ncsu.edu (M. O'Malley).
URLs: http://www.ncsu.edu/math/~gremaud, http://www.math.duke.edu/~jvmatthe.
[1] Partially supported by the National Science Foundation (NSF) through grants DMS-9818900 and DMS-0204578.
[2] Partially supported by the National Science Foundation through grant DMS-9983320.

0021-9991/$ - see front matter © 2004 Elsevier Inc. All rights reserved.
doi:10.1016/j.jcp.2004.04.021

(i) The granular material is modeled as a continuum, with ad hoc constitutive laws.
(ii) The flow is assumed to be steady.
(iii) Only similarity solutions are considered.
(iv) The flow domain is pyramidal, i.e., it is invariant under the transformation (expressed in spherical coordinates) $r \mapsto cr$, for any $c > 0$.
(v) The flow domain is axisymmetric.

The combination of assumptions (iv) and (v) corresponds to a right circular cone, see Fig. 1, upper left

$$\{(r, \theta, \phi) : 0 < r < \infty, 0 \leqslant \theta < \theta_w\}, \quad (\theta_w = \text{constant}). \tag{1}$$

In that case, it was observed by Jenike [12,13] in the late 1950s that similarity solutions, as in (iii), can be constructed (see (8) below for a precise definition). To date, this approach remains a central component in silo design. In [7], restrictions (iii) and (iv) were removed, see Fig. 1, upper right, see also [15,17,19] for more results in that direction. In the present paper, (iii) and (iv) are retained while (v) is removed. More precisely, the hopper is an infinite pyramidal domain

$$\{(r, \theta, \phi) : 0 < r < \infty, 0 \leqslant \theta \leqslant \mathscr{C}(\phi)\}, \tag{2}$$

where $\mathscr{C}$ is a given piecewise smooth 2π-periodic function describing the boundary of the cross section of the hopper, see Fig. 1, bottom left. The present study was started in [9], where *small* perturbations of the axisymmetric case, specifically boundaries of equation $\mathscr{C}(\phi) = \theta_w + \epsilon \cos m\phi$, were considered. Equations for first order corrections in ϵ were derived and solved. Here, cross sections of arbitrary shape can be considered. The authors are aware of no other contribution studying the effects of the geometry on the flow of granular materials in this setting. The case of fully three-dimensional hoppers such as the transitional hopper displayed in Fig. 1, bottom right, appears to be open.

Jenike's solutions are such that grains follow radial lines (only the r-component of the velocity is nonzero). Experimental evidence confirms the important role played by those *radial* solutions in practice [15,16] *in conical containers* (1).

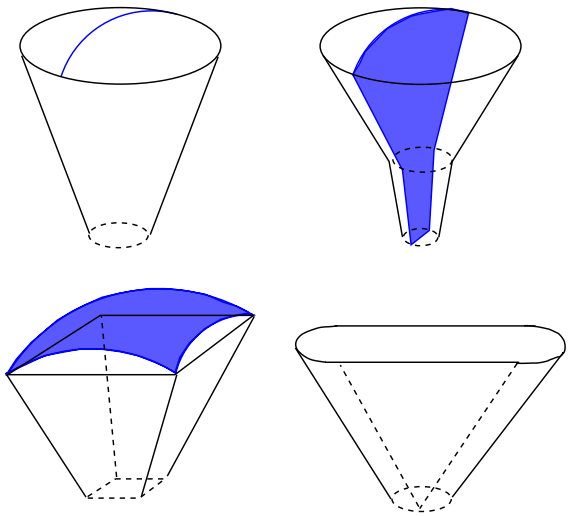

Fig. 1. Various geometries and corresponding numerical domains of resolution; top left: axisymmetric self-similar domain: Jenike's approach on a cone reduces to solving ODEs on a r constant line; top right: axisymmetric non self-similar, see e.g. part I of this series, [7]: nonlinear conservation laws are solved in the shadowed domain; bottom left: nonaxisymmetric self-similar: this paper; bottom right: general three-dimensional hopper: open problem.

Since general pyramidal hoppers are self similar (see (iv)), one could expect the radial character of the flow to hold in those cases as well. Our study, which makes use of assumptions (i) through (iv), finds this to be far from true. We show that a loss of axisymmetry in the hopper geometry induces secondary circulation as well as strong nonuniformity of the stresses in the azimuthal direction.

The paper is organized as follows. The model, geometry, and physical assumptions are discussed in Section 2. Simple scaling arguments reveal the similarity character of the solutions in the r direction. As a result, the solutions are computed on spherical caps of various shapes. The numerical approach is pseudospectral in nature and is described in Section 3. It uses Fourier collocation in longitude and, to account for the boundary conditions, Chebyshev–Gauss–Radau collocation in latitude. Section 4 is devoted to the description of several numerical experiments. Conclusions are offered in Section 5.

2. The model

The physical quantities and corresponding equilibrium equations are expressed in spherical polar coordinates, with the origin corresponding to the vertex of the hopper. For a particular pyramidal domain, a coordinate system that is better suited to the geometry can be constructed. However, such a coordinate system is not typically orthogonal, complicating greatly the structure of the basic equations of Continuum Mechanics [2]. To simplify the numerics, such alternate coordinate systems are introduced in Section 4 through a change of variables, but the individual components of the stress tensor and velocity are still measured with respect to the original spherical coordinates.

The unknowns are the 3×3 symmetric stress tensor T, the 3-component velocity vector v, and a scalar plasticity function λ where

$$T = \begin{bmatrix} T_{rr} & T_{r\theta} & T_{r\phi} \\ T_{r\theta} & T_{\theta\theta} & T_{\theta\phi} \\ T_{r\phi} & T_{\theta\phi} & T_{\phi\phi} \end{bmatrix} \quad \text{and} \quad v = \begin{bmatrix} v_r \\ v_\theta \\ v_\phi \end{bmatrix},$$

(r, θ, ϕ) being the spherical coordinates, with θ the elevation angle and ϕ the azimuthal one. The density ρ is assumed to be constant. In total, there are $3+6+1 = 10$ unknown functions. In writing the equations for these variables, we need the strain rate tensor $V = -(\nabla v + \nabla v^{\mathrm{T}})/2$ and the deviatoric part of the stress tensor $\operatorname{dev} T = T - \frac{1}{3}(\operatorname{tr} T)I$. Note the sign convention: V measures the compression rate of the material; analogously, positive eigenvalues of T correspond to compressive stresses. This sign convention reflects the fact that granular materials disintegrate under tensile stresses.

Following [10,16,22], we require that these variables satisfy

$$\nabla \cdot T = \rho g, \tag{3}$$

$$V = \lambda \operatorname{dev} T, \tag{4}$$

$$|\operatorname{dev} T|^2 = 2s^2 (\operatorname{tr} T/3)^2, \tag{5}$$

where g is the (vector) acceleration due to gravity, $|\cdot|$ denotes the Frobenius norm

$$|T|^2 = \sum_{i,j=1}^{3} T_{ij}^2 = \operatorname{tr} T^2$$

(the latter equality only for symmetric tensors), and $s = \sin\delta$, with δ being the angle of internal friction of the material under consideration (see [16]). Eq. (3) expresses force balance, i.e., Newton's second law with

inertia neglected because the flow is assumed slow; it is equivalent to three scalar equations. Eqs. (4) and (5) are constitutive laws, the alignment condition (or flow rule) and the von Mises yield condition, [3] respectively; they are equivalent to six and to one scalar equations. The full expressions of the equilibrium equation (3) and of V in spherical coordinates are classical and can be found for instance in [23, p. 184]. Thus (3)–(5) is a determined system, 10 equations for 10 unknowns. Since (5) contains no derivatives, this system has a differential-algebraic character. Taking the trace of (4), we see that $\operatorname{div} v = -\operatorname{tr} V = 0$; thus, incompressibility is part of the constitutive assumptions. Incidentally, for a solution to be physical, the function λ in (4) must satisfy $\lambda \geqslant 0$ everywhere; otherwise friction would be adding energy to the system rather than dissipating it. In fact, we want λ to be strictly positive since one of the assumptions underlying the derivation of (3)–(5) is that material is actually deforming.

The alignment condition (4) of the eigenvectors of T and V in effect neglects the rotation of a material element during deformation, a controversial assumption. There is experimental evidence that misalignment may occur under some circumstances [6]. A few alternative models which allow for the above eigenvectors to be somewhat out of alignment have been proposed, see e.g. [24,25]. While such models have been successfully applied to axisymmetric geometries, their formulation becomes very involved in more general cases and has, to our knowledge, never been fully described. Further, there does not seem to be enough experimental data to favor one type of model over the other. We refer to [10] for a lucid, if somewhat dated, account of the situation. Our contribution to this debate is the first calculation of solutions to any model in relatively general geometries. [4]

We seek solutions of (3)–(5) in a pyramidal domain (2). On the boundary $\partial\Omega = \{(r, \mathscr{C}(\phi)), \phi)\}$, wall impenetrability imposes one boundary condition on the velocity: i.e.,

$$v_{\mathrm{N}} = 0, \tag{6}$$

where v_{N} is the normal velocity. Two additional boundary conditions come from Coulomb's law of sliding friction. The surface traction τ – i.e., the force exerted by the wall on the material – is given by

$$\tau_i = \sum_{j=1}^{3} T_{ij} N_j,$$

where N is the unit interior normal to $\partial\Omega$. If the vector τ has normal component τ_{N} and tangential projection $\tau_{\mathrm{T}} = \tau - \tau_{\mathrm{N}} N$, then we require that

$$\tau_{\mathrm{T}} = -\mu_{\mathrm{w}} \tau_{\mathrm{N}} (v/|v|), \tag{7}$$

where μ_{w} is the coefficient of friction between the wall and the material. Note that: (a) If T is positive definite (i.e., if all stresses are compressive), then $\tau_{\mathrm{N}} > 0$. (b) While τ_{N} is a scalar, τ_{T} is effectively a two-component vector; thus, (7) is equivalent to two scalar equations. (c) Because of (6), the velocity v is tangential to $\partial\Omega$; we are assuming that $v \neq 0$ at the boundary.

Putting together assumptions (iii) and (iv) from Section 1, we seek similarity solutions of the form

$$T_{ij} = r \mathscr{T}_{ij}(\theta, \phi), \quad v_i = \frac{1}{r^2} \mathscr{V}_i(\theta, \phi), \quad \lambda = \frac{1}{r^4} \mathscr{L}(\theta, \phi), \tag{8}$$

[3] The name is kept from the corresponding metal plasticity model even though the yield surface is cylindrical there while conical here [22].

[4] Comparison with experimental data is underway; joint work with R.P. Behringer (Duke, Physics), J. Wambaugh (Duke, Physics) and D.G. Schaeffer (Duke, Mathematics). We are also in the process of applying the present approach to materials governed by a Matsuoka–Nakai yield condition [5].

where T_{ij} and v_i are any component of the stress tensor and velocity vector respectively. Eqs. (3)–(5) lead then to the following system for the ten unknowns $\mathscr{T}_{rr}, \mathscr{T}_{r\theta}, \mathscr{T}_{\theta\theta}, \mathscr{T}_{r,\phi}, \mathscr{T}_{\theta\phi}, \mathscr{T}_{\phi\phi}, \mathscr{V}_r, \mathscr{V}_\theta, \mathscr{V}_\phi$ and $\mathscr{L}$.

$$\partial_\theta \mathscr{T}_{r\theta} + \csc(\theta)\partial_\phi \mathscr{T}_{r\phi} + 3\mathscr{T}_{rr} - \mathscr{T}_{\theta\theta} - \mathscr{T}_{\phi\phi} + \cot(\theta)\mathscr{T}_{r\theta} = -\rho g \cos(\theta), \tag{9}$$

$$\partial_\theta \mathscr{T}_{\theta\theta} + \csc(\theta)\partial_\phi \mathscr{T}_{\theta\phi} + 4\mathscr{T}_{r\theta} + \cot(\theta)(\mathscr{T}_{\theta\theta} - \mathscr{T}_{\phi\phi}) = \rho g \sin(\theta), \tag{10}$$

$$\partial_\theta \mathscr{T}_{\theta\phi} + \csc(\theta)\partial_\phi \mathscr{T}_{\phi\phi} + 4\mathscr{T}_{r\phi} + 2\cot(\theta)\mathscr{T}_{\theta\phi} = 0, \tag{11}$$

$$2\mathscr{V}_r = \mathscr{L}(\mathscr{T}_{rr} - \mathscr{P}), \tag{12}$$

$$-\frac{1}{2}(\partial_\theta \mathscr{V}_r - 3\mathscr{V}_\theta) = \mathscr{L}\mathscr{T}_{r\theta}, \tag{13}$$

$$-\partial_\theta \mathscr{V}_\theta - \mathscr{V}_r = \mathscr{L}(\mathscr{T}_{\theta\theta} - \mathscr{P}), \tag{14}$$

$$-\frac{1}{2}(\csc(\theta)\partial_\phi \mathscr{V}_r - 3\mathscr{V}_\phi) = \mathscr{L}\mathscr{T}_{r\phi}, \tag{15}$$

$$-\frac{1}{2}(\partial_\theta \mathscr{V}_\phi + \csc(\theta)\partial_\phi \mathscr{V}_\theta - \cot(\theta)\mathscr{V}\phi) = \mathscr{L}T_{\theta\phi}, \tag{16}$$

$$-(\csc(\theta)\partial_\phi \mathscr{V}_\phi + \mathscr{V}_r + \cot(\theta)\mathscr{V}_\theta) = \mathscr{L}(\mathscr{T}_{\phi\phi} - \mathscr{P}), \tag{17}$$

$$|\mathrm{dev}\,\mathscr{T}|^2 = 2s^2\mathscr{P}^2, \tag{18}$$

where $\mathscr{T} = \frac{1}{r}\mathscr{T}$ and $\mathscr{P} = \frac{1}{3}\mathrm{tr}\,\mathscr{T} = \frac{1}{3}(\mathscr{T}_{rr} + \mathscr{T}_{\theta\theta} + \mathscr{T}_{\phi\phi})$.

The above equations have to be satisfied in the spherical domain $\{(\theta,\phi); -\pi < \phi < \pi <, 0 < \theta < \mathscr{C}(\phi)\}$.

The boundary conditions (6) and (7) can be expressed in terms of the above unknowns. The unit interior normal vector N on the outside wall $\theta = \mathscr{C}(\phi)$ takes the form

$$N = [N_r, N_\theta, N_\phi] = [0, -\sin\theta, \mathscr{C}'(\phi)]\sqrt{\sin^2\theta + \mathscr{C}'(\phi)^2}.$$

Therefore, when $\theta = \mathscr{C}(\phi), 0 < \phi < 2\pi$, one has

$$\mathscr{V}_\theta N_\theta + \mathscr{V}_\phi N_\phi = 0, \tag{19}$$

$$\mathscr{V}_\phi(\mathscr{T}_{r\theta}N_\theta + \mathscr{T}_{r\phi}N_\phi) - \mathscr{V}_r[-\mathscr{T}_{\theta\theta}N_\theta^2 N_\phi + \mathscr{T}_{\theta\phi}N_\theta(1 - 2N_\phi^2) + \mathscr{T}_{\phi\phi}N_\phi N_\theta^2] = 0, \tag{20}$$

$$\begin{aligned}&(\mathscr{T}_{r\theta}N_\theta + \mathscr{T}_{r\phi}N_\phi)^2 + (\mathscr{T}_{\theta\theta}N_\theta N_\phi - \mathscr{T}_{\phi\phi}N_\theta N_\phi + \mathscr{T}_{\theta\phi}(N_\phi^2 - N_\theta^2))^2 \\ &\quad = \mu_w^2(\mathscr{T}_{\theta\theta}N_\theta^2 + 2\mathscr{T}_{\theta\phi}N_\theta N_\phi + \mathscr{T}_{\phi\phi}N_\phi^2)^2,\end{aligned} \tag{21}$$

where (19)–(21) correspond respectively to the conditions (6), $\tau_T \times v = 0$, a vector relation yielding two nontrivial scalar relations, and $|\tau_T| = \mu_w \tau_N$, both expressed in the new variables. Note that the above set of equations defines the unknowns $\mathscr{V}_r$, $\mathscr{V}_\theta$, $\mathscr{V}_\phi$ and $\mathscr{L}$ only up to a multiplicative constant. This is a consequence of the similarity character of the present approach and is found with Jenike's solution as well. To

eliminate this indeterminacy, we fix the value of one component of the velocity, say $\mathscr{V}_r$, at one point in the computational domain. Here, we choose

$$\mathscr{V}_r(\Theta_0, \Phi_0) = v^*, \tag{22}$$

where Θ_0 and Φ_0 are defined in the next section and where v^* in effect scales the flow rate out of the hopper. For Jenike's solution, a typical normalization is to take the maximum (radial) velocity equal to -1. All three one-parameter families of nonaxisymmetric domains considered in Section 4 admit the right circular cone as a special case. In all three cases, the boundary value v^* is taken as the value of Jenike's radial velocity at the wall under the above normalization for a right circular cone. Note that no conditions are needed at $\theta = 0$ (or more precisely, considering only nonsingular solutions at that point is a boundary condition). Further, 2π-periodicity is imposed in the ϕ direction.

Along with the above unknowns, a stream function is also computed. Under assumption (8), the incompressibility condition div $v = 0$ reads here

$$\partial_\theta(\sin\theta \mathscr{V}_\theta) + \partial_\phi \mathscr{V}_\phi = 0.$$

A stream function Ψ can be introduced through

$$\partial_\phi \Psi = \sin\theta \mathscr{V}_\theta, \quad \text{and} \quad \partial_\theta \Psi = -\mathscr{V}_\phi.$$

In fact, Ψ can be characterized as the solution to a Poisson problem on the spherical cap under consideration

$$\Delta\Psi = -\xi_r, \quad \text{for } 0 < \theta < \mathscr{C}(\phi), \ -\pi < \phi < \pi, \tag{23}$$

$$\Psi = 0, \quad \text{on } \theta = \mathscr{C}(\phi), \ -\pi < \phi < \pi, \tag{24}$$

where $\Delta = (1/\sin\theta)\partial_\theta(\sin\theta\partial_\theta) + (1/\sin^2\theta)\partial_{\phi\phi}$ is the Laplace operator on the sphere and ξ_r is r^3 times the r component of the vorticity $\xi = \nabla \times v$, i.e., $\xi_r = \cot\theta \mathscr{V}_\phi + \partial_\theta \mathscr{V}_\phi - (1/\sin\theta)\partial_\phi \mathscr{V}_\theta$. As above, periodicity is assumed in the ϕ direction.

3. Numerical analysis

In order to simplify the numerics, the problem is mapped onto a rectangular computational domain. We define the new coordinates

$$\Theta = \theta_w \frac{\theta}{\mathscr{C}(\phi)} \quad \text{and} \quad \Phi = \phi.$$

Note that $\{\Theta, \Phi\}$ is not an orthogonal coordinate system. However, the computational domain is now simply $(0, \theta_w) \times (-\phi_w, \phi_w)$, where ϕ_w corresponds to the smallest interval of periodicity of the solution in the ϕ direction. More precisely, for a pyramidal hopper of general cross section, $\phi_w = \pi$; for a square cross section for instance, one can take $\phi_w = \pi/4$ and construct the solution from $-\pi$ to π by duplicating the solution obtained between $-\pi/4$ and $\pi/4$ in the obvious way.

Eqs. (9)–(21) are written in the new coordinate system. The reader is spared the expression of the corresponding equations. The resulting problem can be discretized by collocation; Chebyshev collocation at the Chebyshev–Gauss–Radau points is used in Θ, while Fourier-cosine collocation at the Fourier collocation points is used in Φ. Due to the relatively large number of unknowns (ten), the use of a spectral method which delivers high accuracy with a low number of nodes is advantageous, especially since we expect the fields to be smooth. For each of those unknowns, we set

$$U_{NM}(\Theta,\Phi)=\sum_{n=o}^{N-1}\sum_{m=-M/2}^{M/2-1}U_{nm}\psi_n(\Theta)\mathrm{e}^{\mathrm{i}m\pi(\frac{\Phi}{\phi_w}+1)}, \tag{25}$$

where $\{\psi_n\}_{n=0}^{N-1}$ are the Lagrange interpolation polynomials at the Chebyshev–Gauss–Radau nodes on $[0,\theta_w]$, i.e.

$$\Theta_j=\frac{\theta_w}{2}\left(1+\cos\left(\frac{2\pi j}{2N-1}\right)\right),\quad j=0,\ldots,N-1. \tag{26}$$

The above choice, as opposed to the more standard Chebyshev–Gauss–Lobatto collocation, see e.g. [4, Section 2.4], results from the nature of the boundary condition along $\Theta=\theta_w$. For completeness, we derive below the expression of the collocation derivative for Chebyshev–Gauss–Radau nodes (which we have not been able to find in the literature).

Lemma 1. *The Lagrange interpolation polynomials on the Chebyshev–Gauss–Radau nodes* (26) *are given by*

$$\psi_j(\Theta)=\frac{1}{c_j}\frac{\theta_w-\Theta}{\Theta-\Theta_j}\left(\frac{1}{N}T'_N\left(\frac{2\Theta}{\theta_w}-1\right)+\frac{1}{N-1}T'_{N-1}\left(\frac{2\Theta}{\theta_w}-1\right)\right),\quad j=0,\ldots,N-1,$$

where

$$c_0=1-2N,$$

$$c_j=-\frac{\theta_w}{-2\Theta_j}\left(N\cos\frac{2\pi N_j}{2N-1}+(N-1)\cos\frac{2\pi(N-1)j}{2N-1}\right),\quad j=1,\ldots,N-1,$$

and $T_N(x)=\cos(N\arccos x)$, $|x|\leqslant 1$, *is the Chebyshev polynomial of degree N.*

The above result can easily be verified through the use of L'Hospital's rule and elementary properties of the Chebyshev polynomials. Interpolation at the nodes (26) of a function u of Θ defined in $[0,\theta_w]$ simply takes the form

$$I_N u(\Theta)=\sum_{j=0}^{N-1}u(\Theta_j)\psi_j(\Theta).$$

By definition, the Chebyshev collocation derivative of u at those nodes is then

$$(I_N u)'(\Theta_l)=\sum_{j=0}^{N-1}u(\Theta_j)\psi'_j(\Theta_l)=\sum_{j=0}^{N-1}D_{lj}u(\Theta_j),$$

with $D_{lj}=\psi'_j(\Theta_l)$. The collocation derivative at the nodes can then be obtained through matrix multiplication. Elementary albeit tedious calculations lead to the following expressions

$$D_{lj}=\begin{cases}\frac{2}{3\theta_w}N(N-1), & \text{if } l=j=0,\\ \frac{2}{c_0\theta_w\sin 2\frac{2\pi l}{2N-1}}\left(N\cos\frac{2N\pi l}{2N-1}+(N-1)\cos\frac{2(N-1)\pi l}{2N-1}\right) & \text{if } j=0,\ l=1,\ldots,N-1,\\ \frac{c_l}{c_j}\frac{1}{\Theta_l-\Theta_j} & \text{if } j=1,\ldots,N-1,\ j\neq l,\ l=0,\ldots,N-1,\\ -\frac{1}{4\Theta_j}\frac{3\theta_w-2\Theta_j}{\theta_w-\Theta_j}-\frac{\theta_w}{4c_j\Theta_j}\frac{1}{\sqrt{\Theta_j(\theta_w-\Theta_j)}} & \\ (N2\sin(N\arccos(\frac{2\Theta_j}{\theta_w}-1))+(N-1)2\sin((N-1)\arccos(\frac{2\Theta_j}{\theta_w}-1))) & \text{if } j=l=1,\ldots,N-1.\end{cases}$$

To minimize round-off errors, trigonometric identities are used to express the quantities $\Theta_l - \Theta_j$ [20], namely

$$\Theta_l - \Theta_j = \theta_w \sin\left(\frac{\pi}{2N-1}(j+l)\right)\sin\left(\frac{\pi}{2N-1}(j-l)\right), \quad j,l = 0,\ldots,N-1.$$

Further, as suggested in [1], the differentiation matrix D is made to represent exactly the derivative of a constant by numerically satisfying the identity $\sum_{j=0}^{N-1} D_{lj} = 0$, $l = 0,\ldots,N-1$. More precisely, the off-diagonal terms only are computed using the above formula while the diagonal entries are determined by

$$D_{ll} = -\sum_{j=0, j\neq 1}^{N-1} D_{lj}, \quad l = 0,\ldots,N-1.$$

In the Φ direction, the collocation points are taken as the usual Fourier collocation nodes, i.e.,

$$\Phi_l = \phi_w\left(\frac{2l}{M} - 1\right), \quad l = 0,\ldots,M-1. \tag{27}$$

Let U be the $N \times M$ matrix of coefficients U_{nm}, $n = 0,\ldots,N-1$, $m = 0,\ldots,M/2-1,-M/2,\ldots,-1$ for one of the variables under consideration and let W be the $M \times M$ Fourier matrix

$$W = \begin{bmatrix} 1 & 1 & 1 & \ldots & 1 \\ 1 & \omega_M & \omega_M^2 & \ldots & \omega_M^{M-1} \\ 1 & \omega_M^2 & \omega_M^4 & \ldots & \omega_M^{2(M-1)} \\ \ldots & \ldots & \ldots & \ldots & \ldots \\ 1 & \omega_M^{M-1} & \omega_M^{2(M-1)} & \ldots & \omega_M^{(M-1)^2} \end{bmatrix},$$

where $\omega_M = e^{2\pi i/M}$ is the primitive Mth root of unity. Further, if Λ is the $M \times M$ diagonal matrix with diagonal $[0,\ldots,M/2-1,-M/2,\ldots,-1]$, then for any pair j and l, $j = 0,\ldots,N-1$, $l = 0,\ldots,M-1$, the nodal values of U_{NM} and its derivatives can be expressed as follows

$$U_{NM}(\Theta_j,\Phi_l) = (UW)_{jl},$$

$$\partial_\Theta U_{NM}(\Theta_j,\Phi_l) = (DUW)_{jl},$$

$$\partial_\Phi U_{NM}(\Theta_j,\Phi_l) = 4i(U\Lambda W)_{jl}.$$

Each of the ten unknowns $\mathscr{T}_{rr}, \mathscr{T}_{r\theta}, \mathscr{T}_{\theta\theta}, \mathscr{T}_{r\phi}, \mathscr{T}_{\theta\phi}, \mathscr{T}_{\phi\phi}, \mathscr{V}_r, \mathscr{V}_\theta, \mathscr{V}_\phi$ and L is now expanded according to (25). Their coefficient matrices are denoted $U_{rr}, U_{r\theta}, U_{\theta\theta}, U_{r\phi}, U_{\theta\phi}, U_{\phi\phi}, U_r, U_\theta, U_\phi$ and U, respectively. The discretized equations [5] are obtained as follows

- Eqs. (9)–(18), written in terms of (Θ,Φ), are satisfied at the collocation points $\{(\Theta_j,\Phi_l)\}$, $j = 1,\ldots,N-1$, $l = 0,\ldots,M-1$,
- at the boundary nodes $\{\Theta_0,\Phi_l)\}$, $l = 0,\ldots,M-1$, Eqs. (9)–(11) are replaced by the boundary conditions (19)–(21), i.e., Eqs. (12)–(18) and (19)–(21), all written in terms of (Θ,Φ), are satisfied there,
- at (Θ_0,Φ_0), the boundary condition (19) is replaced by (22).

This results in a system of nonlinear equations

$$F(X) = 0,$$

[5] From here on down and unless stated otherwise, we refer to the equations written in the *new* variables (Θ,Φ). As those can easily be obtained from (9)–(21), we do not rewrite them explicitly, for the sake brevity.

where the unknown $X = [U_{rr}, U_{r\theta}, U_{\theta\theta}, U_{r\phi}, U_{\theta\phi}, U_{\phi\phi}, U_r, U_\theta, U_\phi, U]^{\mathrm{T}}$ is a $10N \times M$ matrix and $F : R^{10N\times M} \to R^{10N\times M}$ is a quadratic function with variable coefficients. The current nonlinear solver uses a trust region dogleg method [18] with finite difference Jacobians.

The problem (23) and (24) for the stream function is discretized using the same approach as above, but is solved independently in a post-processing step.

4. Numerical results

Several experiments are presented in order to display the importance of the loss of axisymmetry on the stress and velocity fields. A detailed material parameter study will be presented elsewhere. Note that for ease of interpretation all the numerical results below correspond to values obtained after projection onto a *horizontal* cross section and not a spherical cap as would be directly obtained from the model. The symmetry of both domain and solution is taken into account to reduce computational costs. The discretization is taken as $N = M = 20$; solutions were checked to have converged as expected for spectral methods of this type (i.e., further refinement does not alter the results in any significant way).

4.1. Vertical elliptical hoppers

A family of hoppers described by the following equation are considered

$$\mathscr{C}(\phi) = \frac{\pi/6}{\sqrt{1 - E^2\cos^2\phi}}, \quad 0 \leqslant E < 1, \tag{28}$$

where E stands for the eccentricity. For various eccentricities, the percentage of difference between the largest and smallest values of the normal stress on a horizontal cross section of the wall was computed, see Fig. 2, left. The eccentricity varies from $E = 0$ (circular cross section) to $E = 0.866$ which roughly corresponds to a 2 to 1 ratio between major and minor axes. The relative difference (as a percentage) between the largest and smallest values σ_M and σ_m taken by the normal stress on a horizontal cross section of the wall, i.e., $100\frac{\sigma_M - \sigma_m}{\sigma_m}$ varies correspondingly from 0 (1.81×10^{-11} to be precise) in the axisymmetric case to about

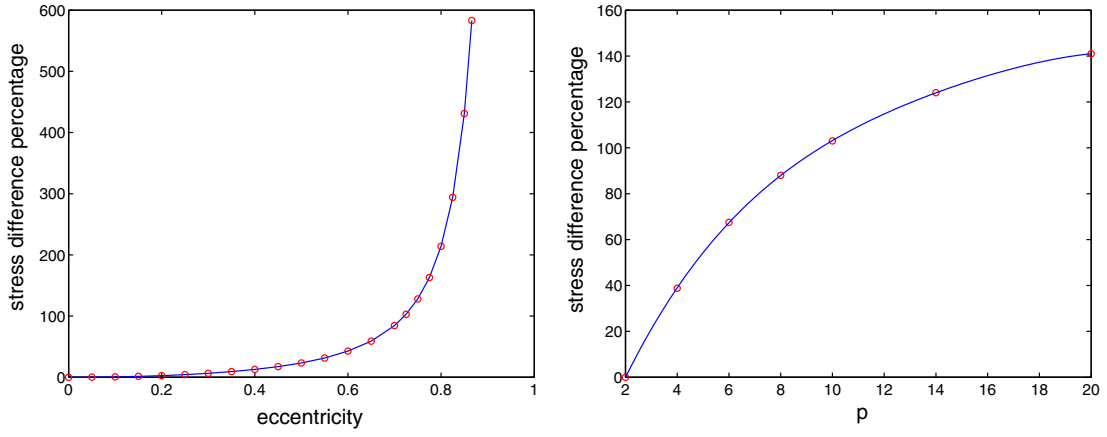

Fig. 2. Effect of the geometry on the normal wall stress. Left: effect of the eccentricity in vertical hoppers with elliptical cross sections given by (28) for E between 0 and 0.866. Right: effect of the parameter p on the normal wall stress in vertical hoppers with square like cross sections given by (29) for p between 2 and 20. Material parameters correspond to corn in a steel hopper: angle of internal friction $\delta = 32.1°$, angle of wall friction $= 11.7°$.

600% for $E = 0.866$. In other words, the normal stress varies by more than a factor 6 for this range of hopper geometries.

Fig. 3 clearly illustrates the effects of the loss of axisymmetry. This is further supported by Fig. 4, which depicts the behavior of the normal stress along the boundary. In the present elliptical case, the normal stress

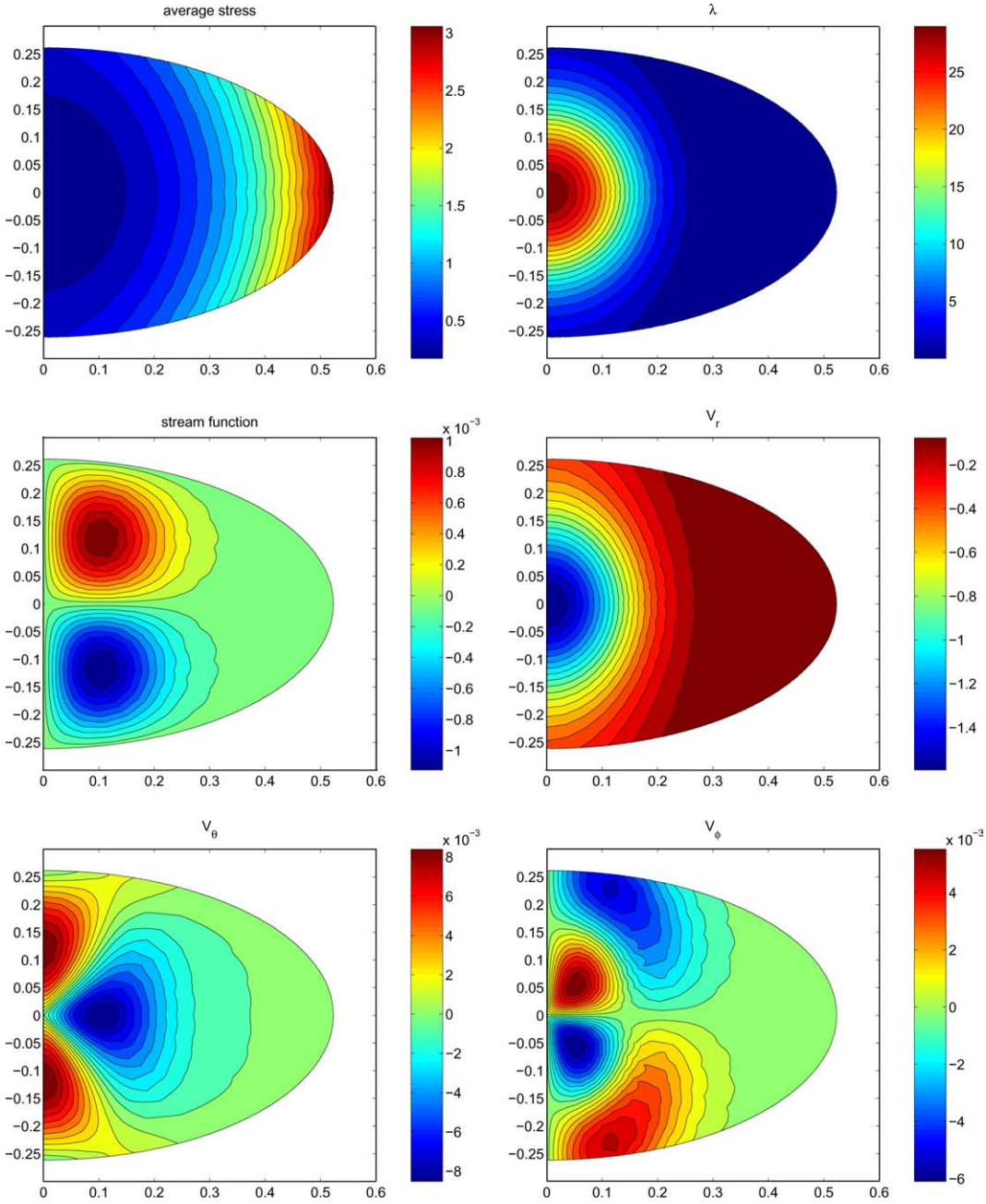

Fig. 3. Flow in a vertical elliptical hopper (28) with $E = 0.866$ (major axis/minor axis ≈ 2); material parameters correspond to corn in a steel hopper: angle of internal friction $\delta = 32.1°$, angle of wall friction $= 11.7°$. Only half of the domain is represented.

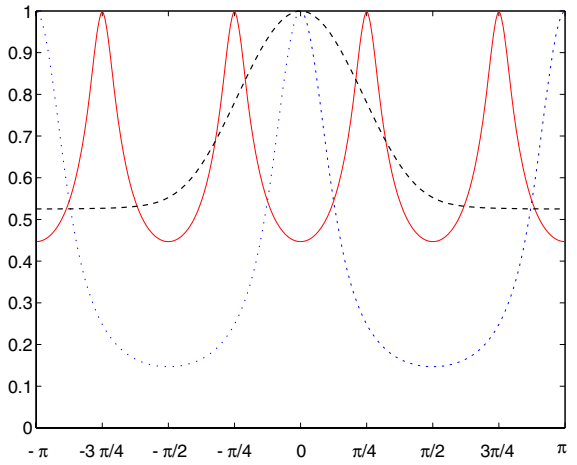

Fig. 4. Behavior of the normal stress along the wall; dash-dot line: vertical elliptical hopper (28) with $E = 0.866$; solid line: vertical "square-like" hopper (29) with $p = 20$; dashed line: tilted right circular hopper (30) with $\theta_w = 30°$ and a tilt angle $\alpha = 14°$; material parameters correspond to corn in a steel hopper: angle of internal friction $\delta = 32.1°$, angle of wall friction = 11.7°. For comparison purposes, the maximal values are normalized to 1.

reaches its maximum value at the points of largest curvature. This type of nonuniformity, while ignored in standard models in this field, may be at the root of very important effects such as shell buckling and other structural failure modes routinely observed in silos [21]. One observes from the graph of $\mathscr{V}_r$ that motion mainly takes place in a central circular core of the domain. Further, secondary circulation, while totally absent from Jenike's theory, is clearly present here as shown by the graph of the stream function: four vortices (for the full domain) are formed. However, the angular components of the velocity, $\mathscr{V}_\theta$ and $\mathscr{V}_\phi$, are about two orders of magnitude smaller than $\mathscr{V}_r$.

4.2. Vertical square hoppers

In spite of being well-known to have suboptimal flowing properties, hoppers with square cross sections are still widely used in many applications.

A family of hoppers described by the following equation are considered

$$\mathscr{C}(\phi) = \frac{\pi/6}{(\cos^p \phi + \sin^p \phi)^{1/p}}, \quad 2 \leqslant p < \infty. \tag{29}$$

The above domain corresponds to the unit disk with respect to the p-norm;for $p \gg 2$, the domain approximates a square.

In Fig. 2, right, the parameter p varies from 2 (circular cross section) to 20. The relative difference (as a percentage) between the largest and smallest values σ_M and σ_m taken by the normal stress on a horizontal cross section of the wall, i.e., $100\frac{\sigma_M - \sigma_m}{\sigma_m}$ varies correspondingly from 0 in the axisymmetric case $p = 2$ to about 150%.

As can be seen from Fig. 4, the nonuniformity of the stresses is less prominent for (almost) square hoppers than it is for elliptical ones. It is worth noting that the normal stress is largest at the corners, a feature of possible importance to structural engineers. The profile of the radial velocity $\mathscr{V}_r$ is much steeper than it was in Fig. 3, a feature reminiscent of funnel flows. Additionally, the angular components of the velocity are here about three orders of magnitude smaller than the radial one; compared to the elliptical

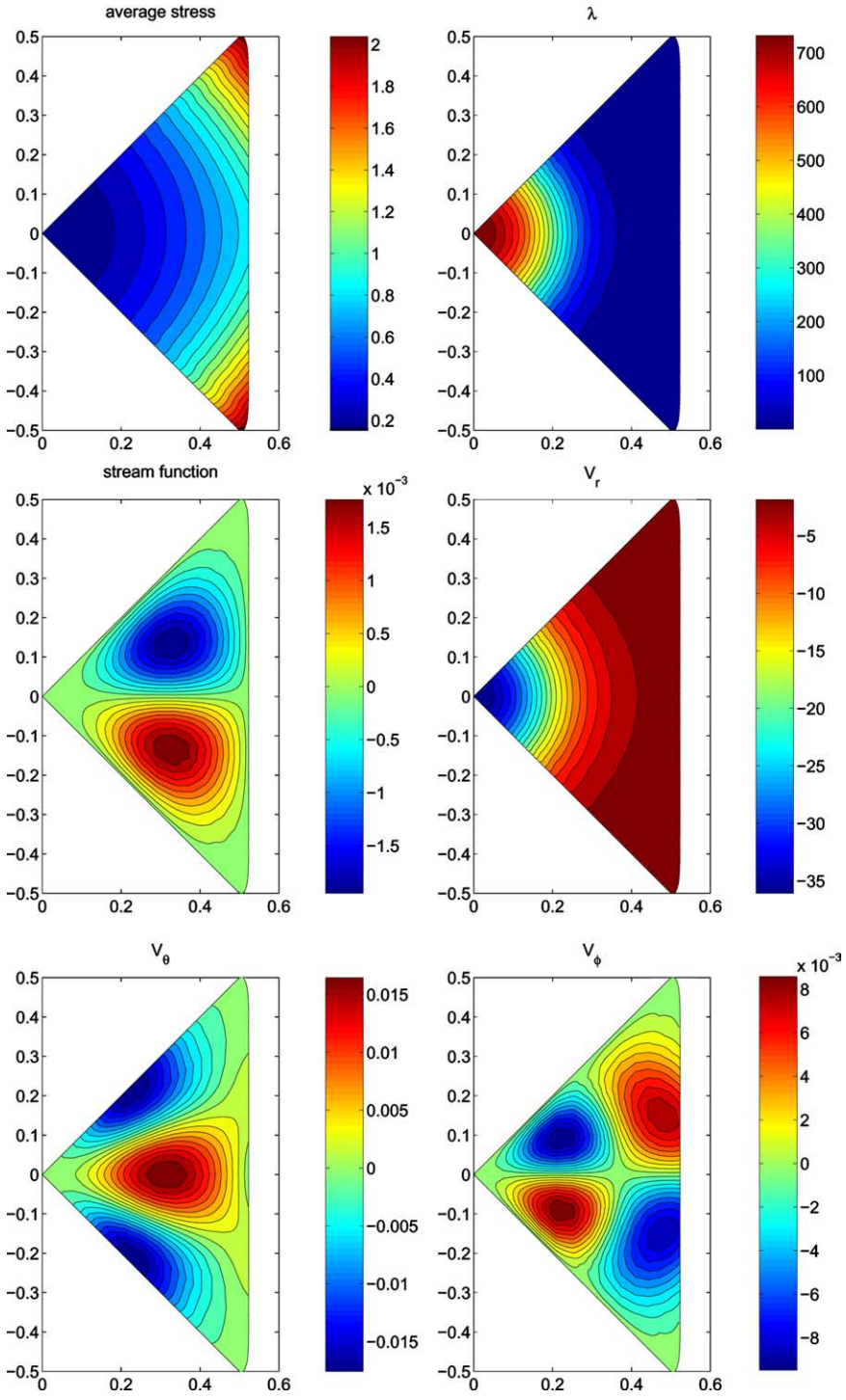

Fig. 5. Flow in a vertical "square-like" hopper (29) with $p = 20$; material parameters correspond to corn in a steel hopper: angle of internal friction $\delta = 32.1°$, angle of wall friction $= 11.7°$. Only a quarter of the domain is represented.

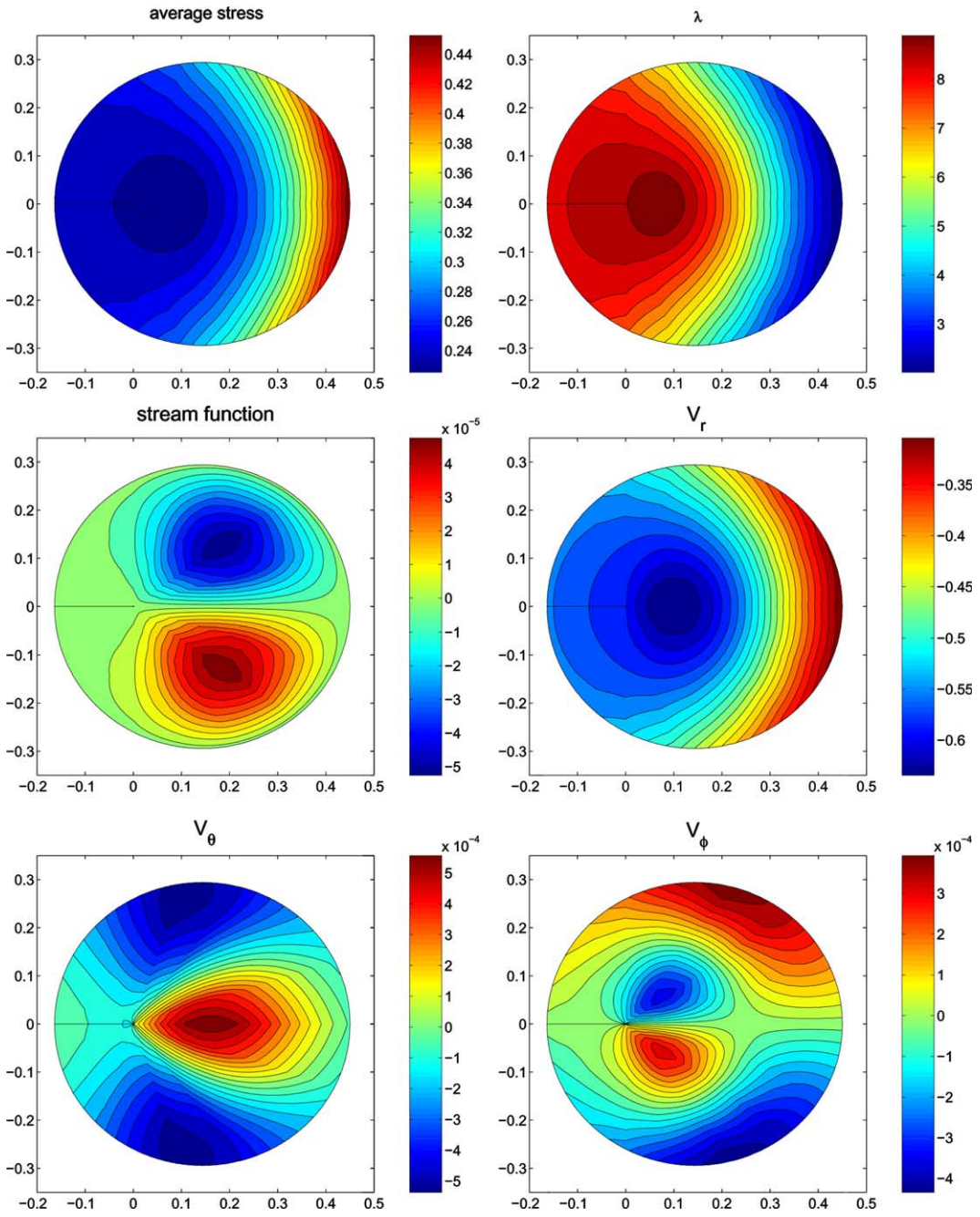

Fig. 6. Flow in a tilted right circular hopper (30) with $\theta_w = 30°$ and a tilt angle $\alpha = 14°$; material parameters correspond to corn in a steel hopper: angle of internal friction $\delta = 32.1°$, angle of wall friction = 11.7°.

hopper, circulation is less pronounced. In the full domain, eight circulation cells are present, as can be seen from the stream function graph in Fig. 5. The structure of the flow does not appear to change significantly for larger values of the parameter p in (29).

Recent experimental results suggest that, in apparent contradiction of Janssen's original prediction [11], the greatest normal stress on the walls of a silo or hopper with square cross-section is felt not at the midpoint of a wall but rather at the corners [3]. Our present computational results seem consistent with these experimental observations.

4.3. Tilted circular hoppers

Industrial applications sometimes call for the use of an off-center outlet at the bottom of a large silo. We consider here the case of tilted right circular cones. More precisely, a right circular cone of (half) opening angle θ_w is tilted in the yz-plane ($\phi \equiv 0$) by an angle α. Elementary trigonometry shows the function $\theta = \mathscr{C}(\phi)$ describing the boundary of the computational domain to be implicitly defined by

$$\cos\theta_w = \sin\alpha \sin\phi \sin\theta + \cos\alpha \cos\theta. \tag{30}$$

Even for relatively small angles of tilt, our numerical experiments show the presence of very steep gradients in some of the unknowns. While this creates computational difficulties, this phenomenon in fact results from the choice of measuring the components of the stress tensor with respect to spherical coordinates. We have verified that, when measured with respect to Cartesian coordinates, the components of the stress tensor are all smooth.

Fig. 6 illustrates the same fields as displayed for the previous two experiments. Only two circulatory cells are observed. The main component of the velocity $\mathscr{V}_r$ is found to be more uniform than in the previous two experiments. The same is true of the average stress and the normal stress on the wall. Fig. 4 shows that the largest value of the normal stress is reached in the direction toward which the hopper is tilted.

5. Conclusions

To our knowledge, this work represents the first time that the present model equations have been solved in three-dimensional nonaxisymmetric geometries. The observed secondary circulation, while predicted in an earlier study of a linearized problem [9], is here fully demonstrated as an effect of the hopper geometry. More importantly, however, this work reveals significant nonuniform stresses, throughout the hopper as well as along the hopper walls. Both results may have practical applications in hopper and silo design and in the prediction of shell buckling.

In particular, the question of the location of greatest normal stress along the outer wall of such nonaxisymmetric hoppers and silos, especially ones of square cross-section, is of great importance. The present contribution is a necessary step toward a comparison of theory with experiments. Further, our approach extends to alternative constitutive laws such as the Matsuoka–Nakai yield condition [5] and may provide insights into which laws best model observations.

Acknowledgements

The authors thank Bob Behringer, Tim Kelley, Michael Rotter, Tony Royal and John Wambaugh for many helpful discussions. They are also grateful to David Schaeffer for many insightful suggestions and remarks without which this paper would not have been possible.

References

[1] A. Bayliss, A. Class, B.J. Matkowsky, Roundoff error in computing derivatives using the Chebyshev pseudo-spectral methods, J. Comput. Phys. 116 (1994) 380383.

[2] L. Brillouin, Les lois de l'élasticité en coordonnées quelconques, Congrés International de Mathématique, Toronto, 1924, Annales de Physique 3 (1925) 251–298.

[3] C.J. Brown, E.H. Lahlouh, J.M. Rotter, Experiments on a square planform steel silo, Chem. Eng. Sci. 55 (2000) 43994413.

[4] C. Canuto, M.Y. Hussaini, A. Quarteroni, T.A. Zang, Spectral Methods in Fluid Dynamics, Springer-Verlag, Berlin, 1988.

[5] I.F. Collins, A systematic procedure for constructing critical state models in three dimensions, Int. J. Solids Struct. 40 (2003) 4379–4397.

[6] A. Drescher, An experimental investigation of ow rules for granular materials using optically sensitive glass particles, Géotechnique 26 (1976) 591–601.

[7] P.A. Gremaud, J.V. Matthews, On the computation of steady hopper flows. I. Stress determination for coulomb materials, J. Comput. Phys. 166 (2001) 63–83.

[8] P.A. Gremaud, J.V. Matthews, M. Shearer, Similarity solutions for granular materials in hoppers, in: J. Bona, K. Saxton, R. Saxton (Eds.), Nonlinear PDE's, dynamics, and continuum physics, Contemporary Mathematics, vol. 255, AMS, 2000, pp. 79–95.

[9] P.A. Gremaud, J.V. Matthews, D.G. Schaeffer, Secondary circulation in granular flow through nonaxisymmetric hoppers, Center for Research in Scientific Computation, NCSU, Technical Report CRSC-TR02-29, to be published in SIAM J. Appl. Math.

[10] R. Jackson, Some mathematical and physical aspects of continuum models for the motion of granular materials, in: R.E. Meyer (Ed.), Theory of Dispersed Multiphase Flow, Academic Press, New York, 1983, pp. 291–337.

[11] H.A. Janssen, Versuche über getreidedruck in silozellen, Zeitschrift des Vereines Deutscher Ingenieure 39 (1895) 1045–1049.

[12] A.W. Jenike, Gravity flow of bluk solids, Bulletin No. 108, Utah Eng. Expt. Station, University of Utah, Salt Lake City (1961).

[13] A.W. Jenike, A theory of flow of particulate solids in converging and diverging channels based on a conical yield function, Powder Technol. 50 (1987) 229–236.

[14] T.M. Knowlton, J.W. Carson, G.E. Klinzing, W.C. Yang, *The importance of storage*, transfer and collection, Chem. Eng. Prog. 90 (1994) 44–54.

[15] J.V. Matthews, An analytical and numerical study of granular flows in hoppers, PhD Thesis, Dept. of Mathematics, North Carolina State Univ., 2000.

[16] R.M. Nedderman, Static and kinematic of granular materials, Cambridge University Press, Cambridge, 1992.

[17] E.B. Pitman, The stability of granular ow in converging hoppers, SIAM J. Appl. Math. 48 (1988) 1033–1052.

[18] M.J.D. Powell, A Fortran Subroutine for solving systems of nonlinear algebraic equations, in: P. Rabinowitz (Ed.), Numerical Methods for Nonlinear Algebraic Equations, 1970 (Chapter 7).

[19] J.R. Prakash, K.K. Rao, Steady compressible ow of cohesionless granular materials through a wedge-shaped bunker, J. Fluid Mech. 225 (1991) 21–80.

[20] E.E. Rothman, Reducing round-off error in Chebyshev pseudospectral computations, in: M. Durand, F. El Dabaghi (Eds.), High Performance Computing II, North-Holland, Amsterdam, 1991, pp. 423–439.

[21] J.M. Rotter, Private Communication, 2003.

[22] D.G. Schaeffer, Instability in the evolution equations describing incompressible granular flow, J. Diff. Eq. 66 (1987) 19–50.

[23] I.S. Sokolnikoff, Mathematical Theory of Elasticity, McGraw-Hill, New York, 1956.

[24] A.J.M. Spencer, Deformation of ideal granular materials, in: H.G. Hopkins, M.J. Sewell (Eds.), Mechanics of Solids, Pergamon Press, New York, 1982, pp. 607–652.

[25] A.J.M. Spencer, Remarks on coaxiality in fully developed gravity flows of dry granular materials, in: N.A. Fleck, A.C.F. Cocks (Eds.), IUTAM Symposium on Mechanics of Granular and Porous Materials, Kluwer, Dordrecht, 1997, pp. 227–238.